Investigation of Accelerated Monte Carlo Techniques for PET Simulation and 3D PET Scatter Correction

C.H. Holdsworth, *Student Member, IEEE*, C.S. Levin*, *Member, IEEE*, T.H. Farquhar, *Student Member, IEEE*, M. Dahlbom, *Senior Member, IEEE*, E.J. Hoffman, *Fellow, IEEE*
UCLA School of Medicine, UCSD School of Medicine* and San Diego VA Medical Center*

Abstract

We have been developing Monte Carlo Techniques for calculating primary and scatter photon distributions in PET. Our first goal has been to accelerate the Monte Carlo Code for fast PET simulation. Our second goal has been to use the simulation to analyze scatter effects in PET and explore the potential for use in scatter correction of clinical 3D PET studies. We have reduced the execution time to about 30 minutes or ~1 million coincidences per minute on a dual 300MHz processor UltraSparcII workstation. The short execution time makes it feasible to use this technique for 3D PET scatter correction in the clinic. Fast simulation also allows us rapid feedback for the close examination of the accuracy of the method. We present techniques used to improve computational efficiency of Monte Carlo PET simulations. We use the simulation to analyze how scatter from within the body, outside the FOV, and from scanner shielding as well as the chosen energy threshold affect 3D PET sinograms.

I. Introduction

To obtain a 5-fold increase in sensitivity, PET scanners can be operated in 3D mode by removing the inter-ring septa. This increases data acquisition rates by allowing additional coincidences along lines of response between non-adjacent detector rings. The cost of the greater sensitivity is an increase in the fraction of random and scatter events and an upper limit on the injected dose due to the difficulties with dead time. In BGO systems currently used, the long scintillation decay time of BGO crystals (300 ns) results in a dead time of greater than a μsec. The lower light output of the crystals has led to a coincidence timing window of 12 ns. As a result, 3D PET thorax imaging using BGO detectors tends to have a lower noise equivalent count rate [1] than comparable 2-D PET studies [2]. When LSO (40 ns decay time and higher light output) PET scanners and a highly accurate scatter correction become available, the performance of 3D PET thorax imaging will be greatly enhanced.

For 2-D PET thorax imaging, one or both photons have been scattered in only 10-20% of all coincidences. This fraction increases to 40%-60% when the septa are removed for 3D PET thorax imaging. This severely degrades image contrast and compromises quantitative accuracy. An accurate scatter correction must be employed before 3D PET can become widely accepted [3,4].

Some scatter corrections are independent of source distribution and attenuating media [5-8]. These methods result in large errors when employed on raw data with a 50% scatter fraction. Activity distribution and attenuation media dependent scatter correction methods show more promise for accuracy [3,4,9-11].

Monte Carlo calculation is "by far the most successful method for the simulation of particle transport in a scattering medium" [12]. The accuracy of Monte Carlo simulations is primarily limited by the accuracy of the input data and the approximations that are utilized in the particular system model. The input data for our Monte Carlo PET simulation is (1) the initial reconstructed PET image, which is used as the activity distribution map, and (2) a segmented attenuation image derived from a short transmission scan taken before or after injection of the isotope, which is the physical attenuation map. The data presented in this paper is the result of simulations of the Siemens/CTI ECAT EXACT HR+ 962 PET system, but any ring geometry can be simulated.

Although variance reduction techniques have been used to reduce computation times in other Monte Carlo Simulations for PET such as PET-EGS [13], PETSIM [14], SimSET [15], and Eidolon [16], these programs are not designed for high speed. They are designed for flexibility, accuracy, and detailed modeling of the physics of the system. Typical execution rates for these PET simulations are on the order of 20-40 ms per acquired event on a Sparc20 workstation for a 3D PET thorax scan [17,18]. This corresponds to a runtime of one or two weeks to acquire 30 million counts. The primary positive result of our work is the significant improvement in the computational efficiency of our simulation program. Our Monte Carlo code currently simulates 80 detected coincidences in 40 ms on a Sparc20 or 700 detected coincidences in 40 ms on a dual processor UltraSparcII. The reduced execution time has allowed us to investigate the effects of scatter in 3D PET using the Monte Carlo approach without having to wait days for each result. We present an accelerated version of a Monte Carlo simulation of 3D PET that can be used for scatter correction [3,4].

II. Materials and Methods

A. Simulation

To evaluate the accuracy of our simulation, we used emission and transmission data with a large number of events

0018-9499/01$10.00 © 2001 IEEE

to minimize noise effects. The Monte Carlo PET Simulation Code was written in C-language. All simulations were run on a 300MHz dual processor Sun UltraSparcII workstation. Although the simulation has 2-D capabilities, all analysis in this paper was achieved using the simulation in 3D mode.

The simulation requires a voxelized activity distribution, which is obtained from the measured emission image volume. We currently use the system's simulation-based scatter correction [10] during reconstruction of the image to provide an initial activity distribution as close to the true distribution as possible.

The simulation also requires a voxelized attenuation map that is obtained from the reconstructed transmission image. Once the attenuation map is reconstructed, the image can be smoothed and segmented to provide a low noise attenuation map [19]. Because the mass attenuation properties of soft tissue and bone are similar in the energy range of our simulation, all voxels are given the same attenuation properties, but different densities are distinguished. Voxels corresponding to lung are smoothed to reduce noise while preserving a distribution of attenuation values. A low threshold value is then used on the attenuation map to set all voxels representing air to zero. As a final step any air voxels that are between two regions with activity and/or positive attenuation values, such as armpits or the space between the subject and patient bed, are assigned a very small nonzero attenuation value. This is done to distinguish photons that have completely escaped all attenuating media, so that these photons can be immediately transported to the detector gantry. This reduces computation time and maintains accuracy.

Once the required data is read into memory, the relative number of annihilations in each voxel is determined by the input emission image. No annihilations are allowed to take place in air. Annihilation photons are transported through the medium using the attenuation map and random numbers to determine locations and results of interactions. If a Compton event occurs, the new direction of the scattered photon is determined using the Klein-Nishina formula and the resulting energy is calculated using the angle of scatter. Once a photon escapes the body, it is transported to the detector gantry. If both detected photons from an annihilation are detected, a 'primary' event is recorded if the energy of both photons is 511 keV, and a 'scatter' event is recorded otherwise. After all annihilations in every voxel of the activity distribution have been simulated, the program generates the scatter and primary sinograms to a file.

B. Phantom

We obtained emission and transmission input for our simulation using a thorax phantom with a major axis of 36.1 cm, a minor axis of 23.1 cm, and an axial length of 26 cm. The phantom contains two 10.3 cm diameter cold lung inserts of density 0.2 gm/ml and a 12.3 cm long cardiac insert in the center of the thorax phantom. The heart has a 10.7 cm diameter cold (no activity) central chamber with 1.2 cm and 1.3 cm thick hot annular chambers about the central chamber. Images of the phantom are shown in figure 1 and 2.

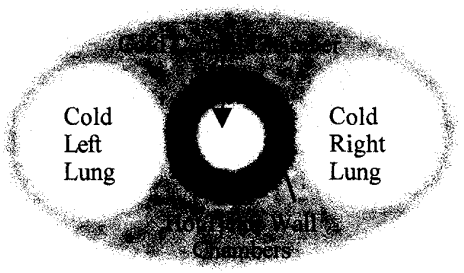

Figure 1. Axial cross-section PET emission image of the thorax phantom used for the activity distribution input to the simulation. Any activity in the lungs or central heart chamber is from scatter.

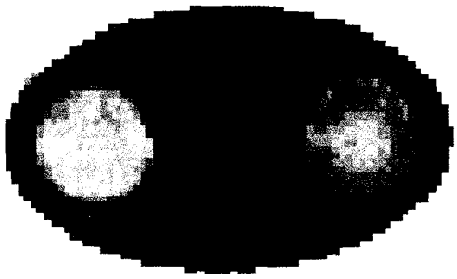

Figure 2. Axial cross-section transmission image of the thorax phantom used for the attenuation map input to the simulation.

C. Assumptions Used in Simulation

In PET studies, photons will often interact at depth in the detector crystals or pass through undetected. To increase the number of detected events in our simulation, any photon hitting a detector's surface is considered detected at that point. Positron range and the non-colinearity of annihilation photons degrade resolution slightly. For increased efficiency, we do not incorporate these effects into our system model. Crystal penetration, crystal scatter, positron range, and non-colinearity will cause only local blurring on the order of a few mm; however, Compton scatter effects in the body can cause much larger positioning errors on the order of the gantry ring radius. Any blurring effects will be washed out in the low frequency scatter distribution. In addition, the resolution of the emission image from which we obtain our activity distribution has already been degraded by these and other effects. So we can ignore these effects with negligible change in the resulting simulated scatter distribution.

Compton scatter contributes to >99% of all annihilation photon interactions above the PET scanner's energy threshold that occur within a patient [20]. Thus, we can neglect the photoelectric effect and coherent scattering without significant loss in accuracy.

Random coincidences depend on the square of the singles count rate of the system, so the amount of random events becomes significant in 3D acquisition. Counts lost to dead time depend on the sensitivity of the system and intensity of the activity distribution. 3D PET is highly sensitive, so dead time limits the amount of activity that can be used in a 3D PET scan and causes a greater portion of events to be lost.

Because the effects of random coincidences and dead time are independent of the scatter distribution, they are ignored in our simulation.

All of these approximations are made in the interest of saving computation time. They can be restored or added, but total run time will be affected.

D. Techniques for Reducing Execution Time

The long execution time of most Monte Carlo Simulations is prohibitive for certain applications and makes its use cumbersome. Other available Monte Carlo simulations would take more than a day to run on an UltraSparcII. Therefore, most of our effort was spent optimizing the code for fast execution. In this section, we present techniques employed to reduce execution time without affecting accuracy.

We began with a few simple, but significant, adjustments to the code to improve computational efficiency. Most PET simulations generate detailed, time-consuming history output files. We were able to reduce execution time by a factor of two by eliminating all output functions that weren't absolutely necessary from our original code [3,4]. We run the program in parallel using both processors on our workstation, cutting the execution time in half. We also tested different optimization compilers and now use the most efficient one. The executable is twice as efficient when it is optimized. After these adjustments were made to the original code [3,4], it was able to simulate a 30 million count 3D PET scan in 12 hours on an UltraSparcII.

The original code used a stratification technique in which only photons within an initial axial acceptance angle limit in the PET gantry would be emitted. This saves the computation time of simulating annihilations in which it is very unlikely that both photons intercept the detector gantry [3,4]. By using an acceptance angle limit of 40° rather than 180°, 4.6 times the number of coincidences are acquired for the same execution time with a 4% loss of scatter events for this phantom. This represents the greatest contribution of error to our code. We plan to address this problem in our future work.

Due to spaces between detectors both axially and transaxially in the Siemens HR+, only about 81% of the gantry surface is actually detector surface, the remaining 19% is space between the detectors. The photons that enter these spaces account for 34% of detected coincidences. By assuming no space between the detectors, all photons hitting the gantry are detected, so we avoid losing these events. This increases efficiency by a factor of 1.5 and will not affect sinogram distributions because the spaces are much smaller than the PET system's resolution and are uniform across the gantry.

Since only coincidence events are recorded, the second photon of an annihilation pair is not simulated if the first photon drops below the energy threshold or is undetected. This shortens the runtime by an additional factor of 1.6.

Computers usually calculate functions such as sine, cosine, etc. using a Taylor Series expansion, which involves multiple operations. By storing values for these functions in arrays with high precision, the calculation can replaced by a single memory access. In addition, the attenuation coefficients for tissue at different energies are also stored in high precision arrays. By implementing this in the code, we achieved an additional factor of 1.5 reduction in execution time with no statistical difference in resulting sinograms (see figure 3).

To further reduce run time, we stored large blocks of random numbers in arrays rather than using a random number generator. In addition, the natural log of random numbers (necessary for photon transport) was stored in a separate array. We currently interweave two separate random number arrays to reduce the possibility of repeating a chain of numbers. To further reduce cyclic effects, the simulation is performed voxel by voxel through the activity distribution, so if a random number sequence is repeated, initial conditions will be different. We compared generated data from simulations with and without tabulated random numbers, and no significant difference could be observed. By tabulating random numbers, computation time is reduced by an additional factor of 1.5. Figure 3 shows the effects on an output sinogram of tabulating the random numbers and various functions.

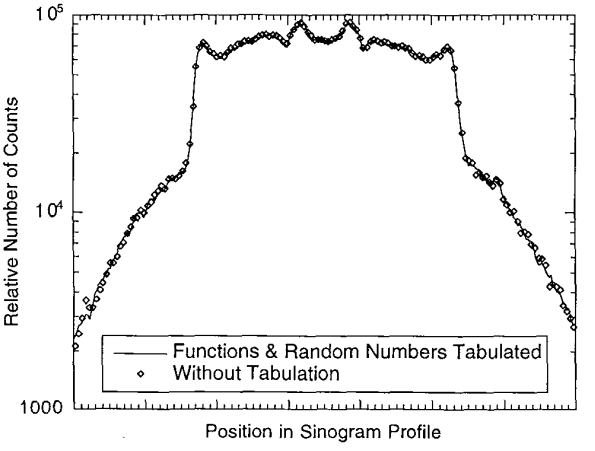

Figure 3. Profiles of a projection plane of simulated totals (scatter + primary events) through the major axis of the thorax phantom with and without tabulation of random numbers and functions. The mean standard deviation of the difference between these two curves is within the 2.0% noise level.

In our original code [3,4], transporting photons took up most of the total computation time. We used a boundary finding method that would step the photon through the attenuation medium to determine the distance to the next boundary. It would then use this distance to determine the probability of interaction and then transport the photon to the appropriate location (boundary edge or point of interaction).

To speed up the code, we developed an interpolation-subtraction method of photon transport that calculates a random attenuation coefficient-distance product, $(\mu \cdot d)_{ran}$. The photon is then stepped through the medium, and the μ-value of each voxel times step distance is subtracted from $(\mu \cdot d)_{ran}$. If $(\mu \cdot d)_{ran}$ reaches zero before the photon exits the body, then an interaction occurs at that point. As photons jump from one voxel to the next, the μ-values of both voxels are averaged to minimize error. Using this method cuts total run time in half.

For even greater efficiency and accuracy, we are currently using the Delta Scattering Photon Transport algorithm [21]. This method transports each photon a random distance assuming the maximum attenuation coefficient for the entire volume. The probability of interaction at the new location is determined by the quotient of that voxel's μ-value divided by the largest μ-value. The photon will continue to be transported in this manner until it escapes the body or its energy falls below a specified threshold. Using this method reduces the run time by a factor of 2.9 over the original method [3,4]. In addition, the delta scattering method is more accurate than either stepping algorithm because there is no error due to the step size. Figures 4 and 5 show that the difference between analytical calculation (using $e^{-\mu x}$) and the delta scattering algorithm used in our simulation is not statistically significant for the noise level of 0.07% in both figures. John DeMarco et al [22] have found similar results. Figure 5 demonstrates the error that occurs at media boundaries when using the stepping algorithm with a 1 cm step size.

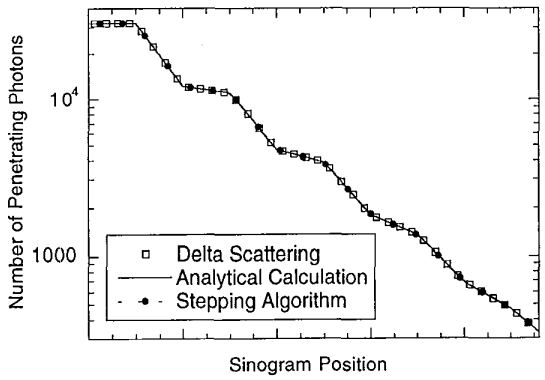

Figure 4. Results of three different methods of simulation of 2 billion photons passing through 100 cm of material comprising a different attenuation value (ranging from 10%-100% that of water) every 10 cm.

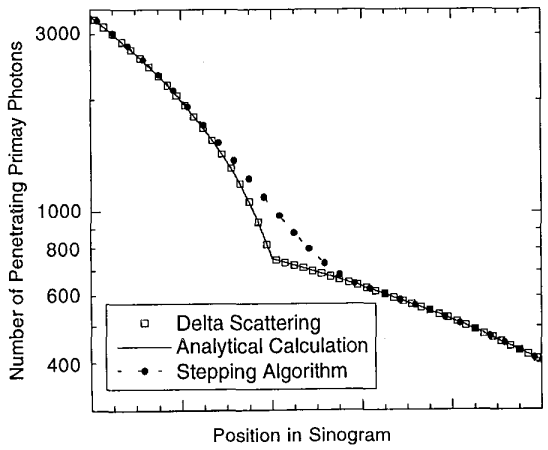

Figure 5. Detailed results at one boundary. The delta scattering graph overlaps with analytical results even on this zoomed scale.

In order to see if all the implementations used to improve computational efficiency had any effect on simulation results, we first had to implement new improvements in accuracy to the older code so there would be no theoretical difference between output sinograms. This includes more accurate attenuation information, more accurate photon transport, attenuation due to the patient bed, and an effective energy threshold that more accurately models the behavior of the system. We ran simulations using the updated code and the modified older version with a high number of counts and summed sinograms over 3 cm axially to reduce effects of noise. We saw no statistically significant difference between simulation sinograms with and without implementation of all improvements in efficiency. Results are shown in figure 6.

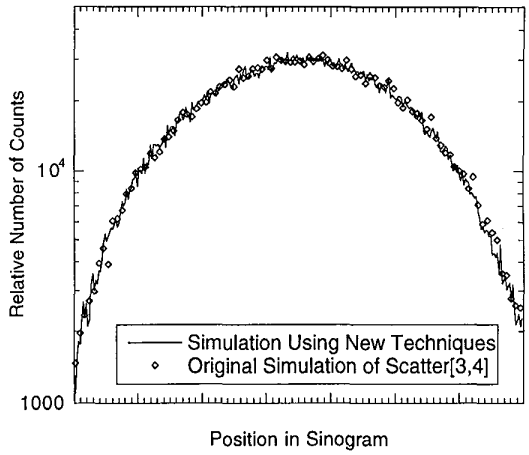

Figure 6. Comparison of the simulated scatter distributions before and after and the new improvements were made on the efficiency of the code. The mean standard deviation of the difference of these sinograms is within the noise level of 2.9%.

Direct application of variance reduction techniques such as forced detection and stratification [24] are not compatible with our method of photon transport. Our program simulates many photons quickly and accurately using the delta scattering algorithm, minimal computation, and uniform photon weight. Most other Monte Carlo simulations force photon detection and calculate appropriate weighting factors. Because the delta scattering transport method samples attenuation values rather than stepping through the attenuation map, weighting factors cannot be calculated efficiently using this technique.

An improvement factor of ~1.3 in the efficiency of the program was the result of many minor adjustments incorporated to streamline the code. Our code currently acquires 30 million coincidences resulting from 600 million annihilations in 30 minutes on an UltraSparcII. This allows us to do multiple simulations per day, and subtle changes in the code can be made and tested quickly, giving rapid feedback on the accuracy of the simulation. Different variables, such as the effect of the energy threshold, can also be studied so that accurate results can be obtained in a short amount of time. The reduced computation time is especially necessary if we want to implement this 3D scatter correction in the clinic.

III. Results

A. Accuracy

Because of the short execution time, we were able to look in detail at energy threshold, axial acceptance angle limit, attenuation map and activity distribution processing, and other variables that might affect the accuracy of the simulation. In this manner we were able to achieve a high level of accuracy while keeping the code as efficient as possible. The current version of the code uses more accurate attenuation information, a more accurate photon transport method, attenuation due to the patient bed, and an effective energy threshold that more accurately models the behavior of the system. Figure 7 compares the original measured image before scatter correction and the simulated totals image. Table 1 shows results of a quantitative analysis of the accuracy of the simulated totals image using the original PET image without scatter correction as the standard. ROI analysis was performed to measure the level of scatter in seven different regions in the thorax images.

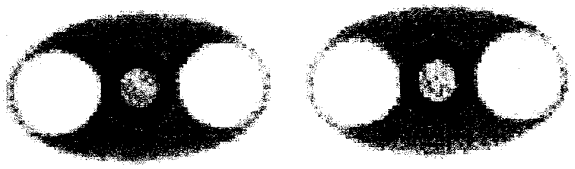

Figure 7. Original Measured Image on left, Simulated Totals Image on right. Note that images contain scatter and primary events.

Table 1. A comparison between the simulated totals image and the original PET image without scatter correction.

Mean ROI Values of Image Intensity		
Location of ROI	Monte Carlo Image of Primary + Scatter	Emission Image with no Scatter Correction
Center of Heart	3.093 ± .069	3.102 ± .060
Outside of Body	0.384 ± .018	0.404 ± .018
Left Lung	0.732 ± .025	0.392 ± .020
Right Lung	0.186 ± .032	0.160 ± .024
Heart Wall	7.197 ± .095	6.961 ± .091
Front of Body	4.153 ± .037	4.145 ± .038
Rear of Body	4.513 ± .027	4.598 ± .026

The higher degree of simulated scatter in the left lung is due to simulation of erroneous lung activity resulting from error in the scanner's scatter correction. This effect disappeared when input activity was not simulated in the lungs. Aside from this effect, ROI analysis shows that the scatter is simulated accurately with a maximum of 3.4% error for different regions in the phantom.

B. Effects of Energy Threshold

Figure 8 shows the effect of different energy thresholds on the simulated total sinograms. Using a lower energy threshold results in a higher scatter fraction and broader distribution. We found that using a lower effective energy threshold of 317 keV gave accurate comparisons between simulated and measured data for this phantom. This threshold was used in figure 7.

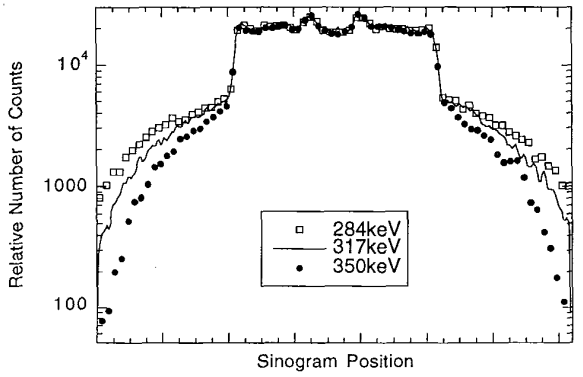

Figure 8. Profiles of a projection plane of simulated totals through the minor axis of the thorax phantom show sinogram differences for the three simulation energy thresholds. The sinograms were summed over 5 cm axially to reduce noise.

Because we have not yet modeled energy response, the effective threshold of 317 keV is significantly lower than 350 keV, which is the nominal energy cutoff used in whole body imaging. We have found a slight dependence in the effective energy threshold of a few keV when using attenuation maps that were significantly larger or smaller than this phantom. This will be addressed in future work.

C. Out of Field of View Scatter and Lead Shielding

Scatter coincidences can result from annihilations that occur outside the axial FOV. The importance of including out of FOV scatter is shown in figure 9. The most obvious discrepancy can be seen just outside the phantom wall.

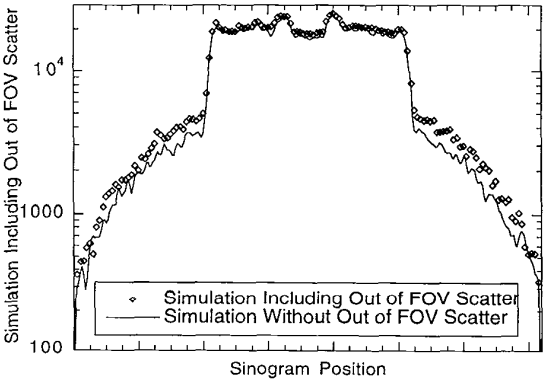

Figure 9. Profiles of a projection plane of simulated totals through the minor axis of the thorax phantom with and without scatter from outside the FOV. The sinograms were summed over 5 cm axially to reduce noise.

Since each simulated annihilation event adds computation time, we do not want to spend time on any activity that does not significantly contribute to the sinograms. It is important

to determine how the significance of annihilations from outside the axial FOV varies with axial position for 3D PET. We simulated rectangular blocks centered in the gantry of uniform activity in water. We varied the width and axial extent of these simulation blocks to see the effect of varying phantom geometry. Figure 10 shows the simulated sensitivity of the scanner to annihilations occurring at different axial positions within the simulated blocks.

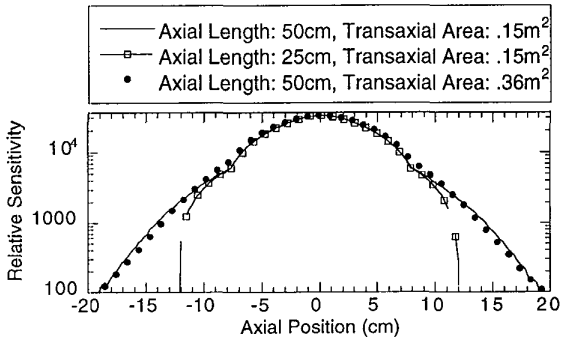

Figure 10. A graph of relative sensitivity versus axial position for different simulated phantom shapes.

The sensitivity is highest at the center of the gantry and falls with distance from the center. A sharp change in the derivative of the curve can be seen at the FOV edge (±7.5 cm). The sensitivity curve for the larger block is slightly higher especially at the edge of the FOV and dips slightly below the curve for the smaller phantom at greater axial distances from the gantry. The sensitivity curve for the block with lesser axial extent falls off drastically near the phantom's axial edge. For the 50 cm long phantoms, ~13% of detected events occurred from activity outside the FOV. ~99% of all detected events result from activity within 7 cm axially of the gantry.

We also studied how transaxial position and attenuation due to the lead shields affect the scatter distribution. The center of a simulation phantom was displaced transaxially from the gantry center by 20 cm. The resulting sensitivity graph versus axial position is included in figure 11. The purpose of the lead shields is to reduce problems with scatter and random events. In figure 11, we include a graph of sensitivity versus axial position for a simulation ignoring the attenuation due to the lead shields.

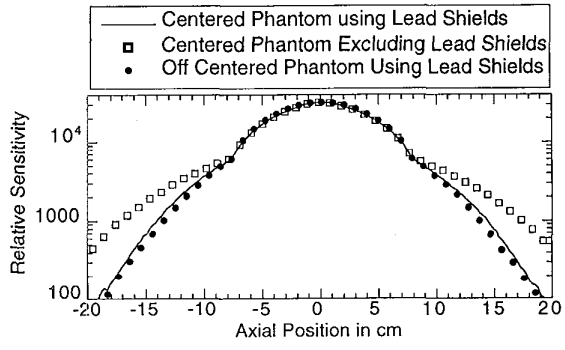

Figure 11. A graph of relative sensitivity versus axial distance.

When the simulation phantom was displaced, the percentage of detected events was slightly higher compared to the centered phantom inside the axial FOV and slightly lower outside the FOV. Without lead shielding, the scanner is more sensitive to activity from outside the FOV. This effect increases with axial distance from the FOV. Our simulation now includes photon attenuation due to the gantry end shields.

The contribution of photon scatter off the lead shields to the scatter distribution is less than 0.5% of all events for the thorax phantom. This effect has little dependence on the shape of the activity distribution, and we have attained similar results for different geometrical configurations. We thus ignore this effect in our current program.

D. Effect of Attenuation by the Patient Bed

The patient bed has a low density; however, it does attenuate a significant amount of photons. In an earlier version of our code [3,4], we did not consider photon attenuation due to the patient bed. Attenuation by the bed causes a significant gradient in the sinogram profile that decreases toward the patient bed. The effect of attenuation through the patient bed is shown in figure 12. Our current code includes this effect.

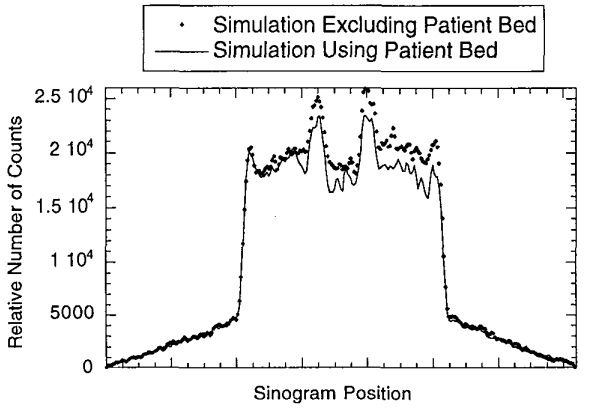

Figure 12. Profiles of a projection plane of simulated totals through the minor axis of the thorax phantom with and without the effect of attenuation by the patient bed. The left and right side of this graph corresponds to the thorax phantom's anterior and posterior regions respectively. Profiles are summed over 5 cm axially to reduce noise.

Because noise in clinical transmission scans can result in significant error in the attenuation map of the bed, we have reconstructed an attenuation image of the bed using data resulting from a very long transmission scan. This information can be used in the attenuation map for any simulated study.

E. Scatter Correction

In order to apply the Monte Carlo Scatter Correction to 3D PET studies in the Clinic, one would first reconstruct the emission data for the activity distribution. We opted to use the scatter correction method already on the system [10] for a best first estimate of the activity distribution. To reduce

processing time, a fast 3D reconstruction technique such as Variable Axial Rebinning using scatter correction would be used to obtain the initial estimate for the activity distribution. The transmission scan would be processed in parallel to obtain the attenuation map (reconstructed in 2-D). The scatter sinogram can then be calculated (currently in 30 minutes) using the Monte Carlo simulation. After subtracting the smoothed and scaled scatter estimate from the original normalized sinogram volume, the resulting sinogram volume can be 3D reconstructed to produce the final image. Thus, the added time of simulation and a fast 3D reconstruction is the time cost of employing the Monte Carlo Scatter Correction.

Figure 13 compares images using CTI's scatter correction and the Monte Carlo scatter correction. Table 2 contains results of a quantitative analysis of these images. ROI values of seven different regions in each image were compared with actual concentrations. The performance of the Monte Carlo scatter correction was comparable or better than CTI's scatter correction in all regions, except for just outside the body. This is due to the non-optimal energy response modeling we are currently using in our simulation. Because we have not yet automated scaling factors for subtraction of the simulated scatter distribution, they were empirically determined for this study. The transmission scan for the thorax phantom was acquired in two hours to reduce effects due to noise in the attenuation information.

Figure 13. Image using CTI's Scatter Correction [10] on left, Image using Monte Carlo Scatter Correction on right.

Table 2. Comparing scatter corrected ROI values with true activity concentrations. Activity concentration values are in μCi/ml.

Location of ROI	Mean ROI Values of Activity Concentration		
	MC Scatter Correction	CTI's Scatter Correction	Activity in Phantom
Center of Heart	0.004 ± .011	0.073 ± .010	0
Outside of Body	0.068 ± .004	0.038 ± .004	0
Left Lung	0.094 ± .005	0.087 ± .005	0
Right Lung	0.050 ± .006	0.062 ± .006	0
Heart Wall	1.388 ± .052	1.414 ± .051	1.4 ± .1
Front Body	0.801 ± .005	0.811 ± .005	0.80 ± .01
Rear Body	0.799 ± .006	0.789 ± .004	0.80 ± .01

* Corrected for Partial Voluming Effects in Respective ROI's.

To reduce the introduction of noise by the scatter correction, smoothing can be employed on the scatter distribution due to its low frequency nature. Currently, we are trying to determine the optimal combination of smoothing algorithm and number of simulated events that will result in an accurate, low noise, and efficient scatter correction.

IV Conclusion

Our Accelerated Monte Carlo Simulation of ECAT HR+ 3D PET scan currently acquires ~1million events per minute. This is 40-80 times faster than other available Monte Carlo PET simulations [17,18] and 24 times faster than our previous code [3,4]. Variance reduction techniques compatible with our code have yet to be implemented. The simulation currently models the original measured distribution to within 3.4%. Most of this error is due to the 40° acceptance angle used in the simulation.

We plan to increase the sophistication of the stratification algorithm by having the acceptance angle depend on position [23]. Using this method, we hope to reduce the error of our model to 1% without any expected loss in computational efficiency. For accurate simulation of different configurations, we are working on a method of incorporating the detection probability for different photon energies that will not sacrifice computational efficiency. This will automatically include effects of energy threshold, energy resolution, and detection efficiency. We are also developing new variance reduction techniques, inspired by techniques used in other Monte Carlo PET simulations [23], that are geared toward our particular approach.

We have demonstrated how the simulation can be used as a tool for analyzing scatter effects in 3D PET studies. In addition, the code is now fast enough that we can look at the effectiveness of employing the simulation as a scatter correction in the clinic. We plan to compare the accuracy of our Monte Carlo scatter correction with other techniques currently available for 3D PET. We also want to study scatter correction performance on phantom distributions with varying noise levels, small animal scanners used for research, and on patient data for clinical 3D PET thorax studies.

V. Acknowledgments

The authors would like to thank Dr. Robert Harrison for valuable discussions on variance reduction techniques, Anthony Daniell for programming advice, and Andrew Goertzen, Dr. Yiping Shao, and Dr. Indrin Chetty for sharing ideas concerning photon transport. This work was funded in part by NCI grant R01-CA56655 and DoE Contract DEF G0387-ER6061.

VI. References

[1] S.C. Strother, M.E. Casey, E.J. Hoffman, "Measuring PET scanner Sensitivity: Relating Count Rates to Image Signal-to-Noise Ratios Using Noise Equivalent Counts," *IEEE Transactions On Nuclear Science*, vol. 37, pp. 783-788, April 1990

[2] T.H. Farquhar, J. Llacer, C.K. Hoh, J. Czernin, S.S. Gambhir, M.A. Seltzer, D.H.S. Silverman, J. Qi, C. Hsu, E. Hoffman, "ROC and localization ROC analyses of lesion detection in whole-body FDG PET: effects of acquisition mode, attenuation correction, and reconstruction algorithm," *Journal of Nuclear Medicine*, vol. 40, p. 2043-2052, December 1999

[3] C.S. Levin, Y. Tai, M. Dahlbom, T.H. Farquhar, E.J. Hoffman, "Removal of the effect of Compton scattering in 3D whole body PET by Monte Carlo", *1995 Nuclear Science Symposium and Medical Imaging Conference Record*, vol. 2, pp. 1050-54, October 1995

[4] C.S. Levin, M. Dahlbom, and E.J. Hoffman, "A Monte Carlo correction for the effect of Compton scattering in 3D PET brain imaging," *IEEE Transactions on Nuclear Science*, vol. 42, pp. 1181-85, August 1995

[5] S. Grootoonk et al, "Correction for Scatter Using a Dual Energy Window Technique with a Tomograph Operating without a Septa", *IEEE Medical Imaging Conference Record*, vol. 3, pp. 1569, 1991

[6] D.L. Bailey and S.R. Meikle, "A Convolution-Subtraction Scatter Correction Method for 3D PET", *Physics in Medicine and Biology*, vol. 39, pp. 411-424, 1994

[7] L. Shao and J.S. Karp, "Cross-Plane Scatter Correction-Point Source De-convolution in PET", *IEEE Transactions on Medical Imaging*, vol. 10, pp. 234, 1991

[8] J.S. Karp et al, "Continuous-slice PENN-PET: A Position Tomography with Volume Imaging Capability", *Journal of Nuclear Medicine*, vol. 31, pp.617-627, 1990

[9] S.R. Cherry, S.R. Meikle, and E.J. Hoffman, "Correction and Characterization of Scattered Events in Three Dimensional PET Using Scanners with Retractable Septa", *Journal of Nuclear Medicine*, vol. 34, pp. 671, 1993

[10] C.C. Watson et al, "Evaluation of simulation-based scatter correction of 3D Cardiac Imaging," *IEEE Transactions on Nuclear Science*, vol. 44, pp. 90-97, February 1997

[11] J.M. Ollinger and G.C. Johns, "Model-based Scatter Correction for Fully 3D PET," *Physics in Medicine and Biology*, vol. 41, pp. 153-176, 1996

[12] H. Chan and K. Doi, Monte Carlo Simulation in Diagnostic Radiology, Boca Raton, FL, CRC Press, 1988, pp. 104-107

[13] I. Castiglioni, O. Cremonesi, M.C. Gilardi, V. Bettinardi, G. Rizzo, A. Savi, E. Bellotti, and F. Fazio, "Scatter correction techniques in 3D PET: a Monte Carlo evaluation," *IEEE Transactions on Nuclear Science*, vol.46, pp. 2053-2058, December 1999

[14] C.J. Thompson, J.M. Cantu, and Y. Piccard, "PETSIM: Monte Carlo program simulation of all sensitivity and resolution parameters of cylindrical positron imaging systems," *Physics in Medicine and Biology*, vol. 37, pp. 731-749, 1992

[15] M.S. Kaplan, R.L. Harrison, and S.D. Vannoy, "Coherent Scatter Implementation for SimSET," *IEEE Transactions on Nuclear Science*, vol.45, pp. 3064-3068, December 1998

[16] H. Zaidi, A Scheurer, and C. Moral, "An object-oriented Monte Carlo simulator for 3D positron tomographs," Computer Methods and Programs Biomedcine, vol. 58, pp. 133-145, 1999

[17] Communication with I. Castiglioni, "The MC-PET Project: Building an open-to-public Database of Monte Carlo Data sets for PET," Society of Nuclear Medicine Annual Meeting Program, pp. 132, 2000

[18] H. Zaidi, "Relevance of accurate Monte Carlo modeling in nuclear medical imaging," *Medical Physics*, vol. 26, pp. 574-608, April 1999

[19] S.R. Meikle, M. Dahlbom, and S. Cherry, "Attenuation correction using count-limited transmission data in Positron Emission Tomography," *Journal of Nuclear Medicine*, vol. 34, pp.143-150, January 1993

[20] H.E. Johns and J.R. Cunningham, The Physics of Radiology, Springfield, IL, Charles C Thomas, 1983, pp. 723-33

[21] E.R. Woodcock et al, "Techniques Used in the GEM Code for Monte Carlo Neutronics Calculation", *Proceeding on the Conference for Applications of Computing Methods to Reactors*, ANL-7050, pp. 557, 1965

[22] J.J. DeMarco, T.D. Solberg, I. Chetty, J.B. Smathers, "Efficient sampling algorithms for Monte Carlo based treatment planning," *Radiation Physics and Chemistry*, vol. 53, pp. 229-234, 1998

[23] D.R. Haynor, R.L.Harrison, et. al, "Improving the Efficiency of Emission Tomography Simulations Using Variance Reduction Techniques," *IEEE Transactions on Nuclear Science*, vol. 37, pp. 749-753, April 1990

[24] P.E. Kinahan and J.G. Rogers, "Analytic 3D image reconstruction using all detected events," *IEEE Transactions on Nuclear Science*, vol. 36, pp. 964-68, 1989

[25] J.G. Colsher, "Fully three-dimensional positron emission tomography," *Physics in Medicine and Biology*, vol. 25, pp. 103-15, 1980

[26] S.R. Cherry, M. Dahlbom, and E.J. Hoffman, "Evaluation of a 3D reconstruction algorithm for multi-slice positron emission tomography scanner," *Physics in Medicine and Biology*, vol. 37, pp. 779-790, 1992

Send Correspondence To:
Clay Holdsworth
10833 Le Conte Avenue
B2-086 CHS
Los Angeles, CA 90095
choldsworth@mednet.ucla.edu